

Shape coexistence and isomeric states in ^{94}Pd within a beyond-mean-field approach

A. S. Mare  and A. Petrovici *

Horia Hulubei National Institute for Physics and Nuclear Engineering, R-077125 Bucharest, Romania
and Faculty of Physics, University of Bucharest, R-077125 Bucharest, Romania



(Received 29 June 2022; accepted 21 October 2022; published 3 November 2022)

The evolution of shape coexistence and mixing in the structure of ^{94}Pd positive parity states and the nature of the isomeric states at spin 8^+ and 14^+ are self-consistently studied within the beyond-mean-field *complex* excited Vampir model using an effective interaction derived from a nuclear matter G matrix based on the charge-dependent Bonn CD potential in a large model space. Within the same theoretical framework we investigated the Gamow-Teller β decay of the 7^+ isomer and the superallowed Fermi β decay of the 0^+ ground state of ^{94}Ag to ^{94}Pd . Results on the structure and electromagnetic properties of positive parity states up to spin 14^+ in ^{94}Pd as well as the strength distributions for the ^{94}Ag β decay feeding the investigated states in ^{94}Pd are discussed and compared with the available experimental data.

DOI: [10.1103/PhysRevC.106.054306](https://doi.org/10.1103/PhysRevC.106.054306)

I. INTRODUCTION

The heaviest nuclei around the $N = Z$ line up to the doubly magic ^{100}Sn are intensively studied both experimentally and theoretically due to the open questions concerning the nature of the observed isomeric states and irregularities in the excitation spectra as well as the relevance for astrophysical scenarios concerning the rp -process path [1–13]. The exotic structure and dynamics of these nuclei are expected to be generated by the interplay between competing $T = 0$ and $T = 1$ proton-neutron and like-nucleon pairing correlations, isospin-symmetry-violation interactions, and shape coexistence and mixing. Previously various types of shell-model calculations have been employed in order to describe the nuclear properties of isotopes around the $N = Z = 50$ line: shell-model calculations using empirical effective interactions in a restricted ($1p_{1/2}, 0g_{9/2}$) model space and large-scale shell-model calculations using larger model spaces including excitations across the ^{100}Sn shell closure [14–20].

Coexistence phenomena in $N \approx Z$ nuclei in the $A = 60$ – 90 mass region have been described previously using different models [21–28]. A challenge for theory is the simultaneous description of the properties of low- and intermediate-spin states including the nature of the isomers and β decay feeding of these states from the neighboring nuclei.

This work represents the extension of the investigations within the beyond-mean-field *complex* excited Vampir variational model to the proton-rich nuclei with mass above 90. This study is an attempt at a comprehensive understanding of the effects of shape coexistence and mixing on the isomeric states in ^{94}Pd and the properties of the β decay of the 7^+ isomer and the 0^+ ground state of ^{94}Ag feeding the daughter states in ^{94}Pd within the same theoretical framework.

The next section presents the main theoretical ingredients of the beyond-mean-field *complex* excited Vampir variational model. In Sec. III we discuss the results concerning shape coexistence and mixing effects on the structure and electromagnetic properties of positive parity states up to spin 14^+ in ^{94}Pd and the feeding of investigated states by the β decay of the 7^+ isomer and the 0^+ ground state of ^{94}Ag . Final remarks and conclusions are drawn in Sec. IV.

II. THEORETICAL FRAMEWORK

The *complex* excited Vampir model (EXVAM) uses Hartree-Fock-Bogoliubov (HFB) vacua as basic building blocks. The underlying HFB transformations are essentially complex and allow for proton-neutron, parity, and angular momentum mixing being restricted by time-reversal and axial symmetry. Using essentially complex unitary transformations creates the possibility to account for natural- and unnatural-parity two-body correlations as well as $T = 1$ and $T = 0$ neutron-proton pairing correlations already at the mean-field level. The broken symmetries, nucleon number, total angular momentum, and parity are restored before variation using projection techniques. The symmetry projected configurations are used as trial wave functions in chains of successive variational calculations for each specific symmetry. The HFB transformations and the configuration mixing are determined within the variational procedure behind the *complex* excited Vampir model ([26] and references therein).

For nuclei around the $N = Z$ line we use above the ^{40}Ca core a model space including the $1p_{1/2}, 1p_{3/2}, 0f_{5/2}, 0f_{7/2}, 1d_{5/2}$, and $0g_{9/2}$ oscillator orbits for both protons and neutrons in the valence space. Using this model space we have successfully described shape coexistence phenomena revealed by the structure and allowed β decay of $N \approx Z$ $A = 60$ – 90 nuclei [21,26,27]. Starting with an isospin-symmetric basis, Coulomb shifts for the proton single-particle levels induced

*spetro@nipne.ro

TABLE I. The amount of mixing for the *complex* excited Vampir states presented in Fig. 1. The contributions (of at least 2%) of EXVAM configurations are indicated in decreasing order.

$I (\hbar)$	Oblate content	Prolate content
0_1^+	91(4)%	4%
0_2^+	86%	10%
2_1^+	23(3)%	73%
2_2^+	71%	24(3)%
4_1^+	2%	93(3)%
4_2^+	53(2)%	40(4)%
6_1^+	9(2)%	87%
6_2^+	67(16)(5)%	7(5)%
6_3^+	29(28)(20)(2)%	13(4)(3)%
8_1^+	77(7)%	9(5)%
8_2^+	66(15)(3)%	16%
8_3^+	23(3)%	72%
10_1	23(9)%	64%
12_1^+	59(22)%	14(2)%
14_1^+	95(2)%	

by the ^{40}Ca are obtained by spherically symmetric Hartree-Fock calculations involving the Gogny-interaction DIS in a 21 major-shell basis [26]. The effective two-body interaction is constructed from a nuclear matter G matrix based on the charge-dependent Bonn CD potential. To enhance the pairing correlations the G matrix was modified by adding short-range Gaussians in the $T = 1$ and $T = 0$ channels. To influence the onset of deformation and the prolate-oblate competition, monopole shifts of -500 keV for the $T = 0$ matrix elements of the form $\langle 1p1d_{5/2}; IT = 0 | \hat{G} | 1p1d_{5/2}; IT = 0 \rangle$ ($1p$ denotes either the $1p_{1/2}$ or the $1p_{3/2}$ orbital) and of -275 keV for $\langle 0g_{9/2}0f; IT = 0 | \hat{G} | 0g_{9/2}0f; IT = 0 \rangle$ ($0f$ denotes either the $0f_{5/2}$ or the $0f_{7/2}$ orbital) were added. The shifts for the latter matrix elements have been varied from -250 to -400 keV within the investigations of $A = 60-90$ proton-rich nuclei. The Hamiltonian includes the two-body matrix elements of the Coulomb interaction between the valence protons.

III. RESULTS AND DISCUSSION

A. The 8^+ and 14^+ isomers in ^{94}Pd

For the investigation of the even-spin positive parity states up to spin 14^+ in ^{94}Pd , ten orthogonal many-nucleon *complex* excited Vampir configurations were constructed for each considered symmetry. By diagonalizing the residual interaction between the states that form the many-body basis for a given symmetry, the mixing of the differently deformed projected configurations in the intrinsic system in the structure of the wave functions is obtained. The evolution of the shape coexistence and mixing with increasing spin and excitation energy is illustrated by the structure of the wave functions for the investigated states. The prolate-oblate mixing for the states building the yrast band, the first excited band, and the second excited 6^+ and 8^+ states is presented in Table I, indicating the contributions of the EXVAM configurations bringing at

TABLE II. The spectroscopic quadrupole moments (in $e\text{fm}^2$) for positive parity EXVAM states in ^{94}Pd .

$I (\hbar)$	Q	$I (\hbar)$	Q
2_1^+	-9.5	8_1^+	50.4
2_2^+	12.4	8_2^+	36.8
4_1^+	-37.5	8_3^+	-8.9
4_2^+	1.5	10_1^+	15.3
6_1	-28.9	12_1^+	8.3
6_2^+	36.3	14_1^+	45.6
6_3^+	19.1		

least 2% to the total amplitude. The lowest two 0^+ states are dominated by oblate deformed configurations in the intrinsic system, while the third 0^+ is dominated by a prolate deformed one. The yrast 2^+ , 4^+ , and 6^+ states are dominated by prolate deformed configurations, while the corresponding first excited states indicate dominant oblate content, with maximum oblate-prolate mixing characterizing the second 4^+ state. Very strong mixing of differently deformed oblate and prolate configurations was found for the third 6^+ state. At spin 8^+ the structure of the wave function is changed, the yrast 8^+ state being dominated by oblate components, as is the case for the second 8^+ state, too, while the third one is dominated by a prolate deformed configuration. Up to spin 8^+ the quadrupole deformation parameter varies from $\beta_2 = 0.07$ to $\beta_2 = 0.14$ for the prolate deformed EXVAM configurations, while for the oblate deformed ones it varies from $\beta_2 = -0.07$ to $\beta_2 = -0.17$. With increasing spin the quadrupole deformation is decreasing. Thus for the 10^+ , 12^+ , 14^+ spin states the deformation parameter displays values from $\beta_2 = 0.03$ to $\beta_2 = 0.10$ and from $\beta_2 = -0.03$ to $\beta_2 = -0.14$ for prolate and oblate EXVAM configurations, respectively. As illustrated in Table I, the yrast 10^+ state manifests strong oblate-prolate mixing, while the 12^+ and 14^+ yrast states indicate dominant oblate content. The effects of the prolate-oblate mixing are reflected in the spectroscopic quadrupole moments of the investigated states which are illustrated in Table II. Based on the available experimental information in the region, effective charges of $e_p = 1.3$ and $e_n = 0.3$ have been used.

Figure 1 illustrates the EXVAM spectrum constructed based on the $B(E2)$ values connecting the states compared to the experimental data [29]. Full lines in the theoretical spectrum indicate $B(E2; I \rightarrow I - 2)$ transitions. The calculated $B(E2; I \rightarrow I - 2)$ values for the yrast and first excited band are shown in Table III. Recent experimental results [20] confirming the isomeric character of the yrast 8^+ and 14^+ states [19,30] present new values for the corresponding half-lives, $T_{1/2}^{exp}(8^+ \rightarrow 6^+) = 1.2(3)$ ns and $T_{1/2}^{exp}(14^+ \rightarrow 12^+) = 499(9)$ ns. The calculated EXVAM $B(E2)$ values for the isomers indicate good agreement with the experimental data: we have obtained for the $B(E2; 8^+ \rightarrow 6^+)$ strength the value $165 e^2\text{fm}^4$, while the experimental value amounts to $130(30) e^2\text{fm}^4$ [20]; and for the $B(E2; 14^+ \rightarrow 12^+)$ strength the value of $56 e^2\text{fm}^4$, while the experimental value is $53(1) e^2\text{fm}^4$ [20]. Shell-model calculations carried out using

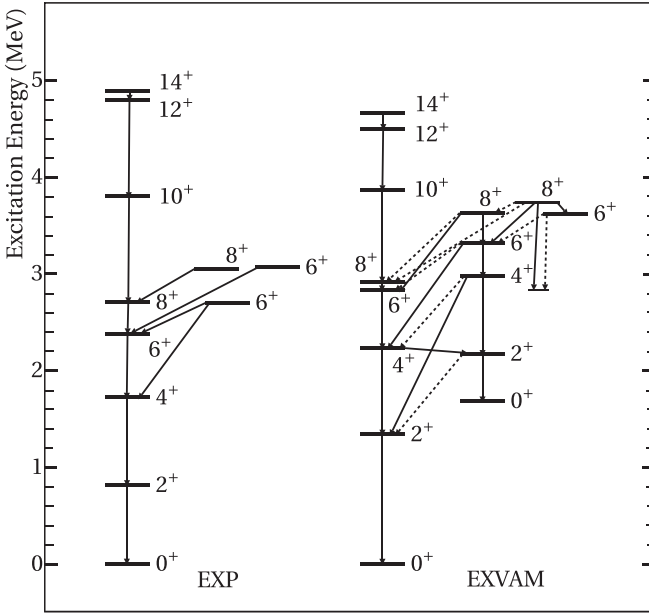


FIG. 1. The *complex* excited Vampir spectrum for ^{94}Pd compared with experimental data [29] (see text for explanations).

the Gross and Frankel (GF) [14] or the Jun45 [22] interaction achieved good agreement with the experimental $B(E2)$ values for the 8^+ and 14^+ isomers [20]. Shell-model results obtained using the empirical GF interaction compares well to the experimental spectrum [17].

The decay pattern of the lowest three 6^+ and the lowest two 8^+ states in the EXVAM spectrum compares well with experimental data. In Table IV we present the $B(E2)$ and $B(M1)$ transition strengths for the decay of the lowest three 8^+ and 6^+ states in ^{94}Pd . The EXVAM results indicate significant $E2$ and $M1$, $\Delta I = 0$ transitions connecting the lowest three 6^+ as well as 8^+ states. Strong $M1$ transitions were obtained for the decay of the second 8^+ state and the third 8^+ state as well as a significant $E2$ branch connecting the third and the yrast 8^+ state. Significant $M1$ transition strengths have been obtained for the decay of the second and the third 6^+ states. The second and the first 4^+ states are connected via an $M1$ branch of $0.18\mu_B^2$ strength and an $E2$ branch of $32 e^2\text{fm}^4$ strength. The lowest two 2^+ states are linked by

TABLE III. $B(E2; I \rightarrow I - 2)$ values (in $e^2\text{fm}^4$) for the yrast and first excited band presented in Fig. 1. The strengths for secondary branches are given in parentheses. The strengths given in square brackets are not shown in the figure.

I (\hbar)	Yrast band	First excited band
2^+	367	426
4^+	383 (81)	213 (104)[134]
6^+	336 [105]	240 (99)
8^+	165 [60][111]	118 (31)[51]
10^+	278 [34]	
12^+	160 [32]	
14^+	56	

TABLE IV. $B(E2)$ (in $e^2\text{fm}^4$) and $B(M1)$ (in μ_B^2) transition strengths for the decay of the lowest three 8^+ and 6^+ states in ^{94}Pd .

Transition	$B(E2)$	$B(M1)$
$6_2^+ \rightarrow 6_1^+$	103	0.62
$6_3^+ \rightarrow 6_1^+$	99	0.26
$6_3^+ \rightarrow 6_2^+$	37	0.75
$8_1^+ \rightarrow 6_1^+$	165	
$8_2^+ \rightarrow 6_1^+$	31	
$8_2^+ \rightarrow 6_2^+$	118	
$8_2^+ \rightarrow 8_1^+$	61	3.07
$8_3^+ \rightarrow 6_1^+$	159	
$8_3^+ \rightarrow 6_2^+$	44	
$8_3^+ \rightarrow 6_3^+$	67	
$8_3^+ \rightarrow 8_1^+$	128	0.41
$8_3^+ \rightarrow 8_2^+$	82	3.97

a strong $E2$ transition of $364 e^2\text{fm}^4$ strength. Shell-model calculations of the $B(E2)$ and $B(M1)$ strengths connecting the states populated in the β decay of the 7^+ isomer in ^{94}Ag were carried out [18]. Using the GF empirical interaction good agreement with the data was found for the lowest few 6^+ and 8^+ states. Large-scale shell-model calculations performed by the same authors in the gds model space comprising the $0g_{9/2}$, $0g_{7/2}$, $2s_{1/2}$, $1d_{5/2}$, and $1d_{3/2}$ orbitals for protons and neutrons predict the same sequence of the lowest few 6^+ and 8^+ states as the one obtained using empirical shell-model calculations. Also good agreement with the $B(E2)$ experimental value for the 14^+ isomer is reported [18].

It is worthwhile to mention that support for the shape coexistence and mixing revealed by the structure of the wave functions is offered by the $E0$ transitions connecting not only the lowest few 0^+ states, but also the lowest few calculated 2^+ states, as illustrated in Table V.

The evolution in the structure of the investigated states is also revealed by the neutron and proton occupations of the $1p_{1/2}$, $1p_{3/2}$, $1d_{5/2}$, and $0g_{9/2}$ valence spherical orbitals for the yrast band and the lowest three 6^+ and 8^+ states illustrated in Figs. 2 and 3, respectively. Particular changes can be observed in the occupation of the $0g_{9/2}$, $1p_{1/2}$, and $1p_{3/2}$ orbitals for both protons and neutrons at the 8^+ isomer, but not for the 14^+ isomer. Significant changes in these occupations are observed

TABLE V. $\rho^2(E0)$ values for the lowest few 0^+ and 2^+ states in ^{94}Pd .

Transition	EXVAM
$\rho^2(E0; 0_2^+ \rightarrow 0_1^+)$	0.019
$\rho^2(E0; 0_3^+ \rightarrow 0_1^+)$	0.007
$\rho^2(E0; 0_3^+ \rightarrow 0_2^+)$	0.005
$\rho^2(E0; 2_2^+ \rightarrow 2_1^+)$	0.022
$\rho^2(E0; 2_3^+ \rightarrow 2_1^+)$	0.011
$\rho^2(E0; 2_3^+ \rightarrow 2_2^+)$	0.008

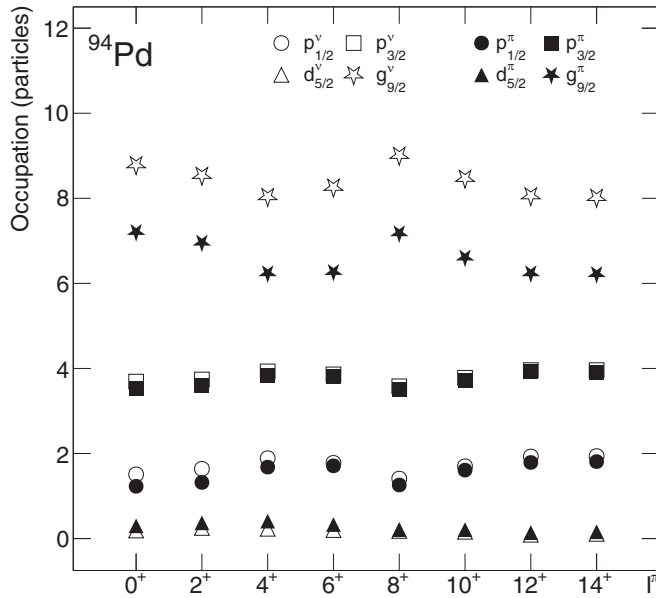


FIG. 2. Occupation of the $1p_{1/2}$, $1p_{3/2}$, $1d_{5/2}$, and $0g_{9/2}$ valence spherical orbitals for the yrast band in ^{94}Pd .

comparing the evolution for the lowest three 6^+ states as well as for the lowest three 8^+ states.

The alignment plot representing the angular momentum contributions of the nucleons occupying the $0g_{9/2}$ orbital in the direction of the total angular momentum for the yrast band and the first excited band is presented in Fig. 4. In the yrast band the plot indicates a fast alignment of the protons and a small contribution brought by the neutrons at low spins followed by an increased proton alignment and simultaneously a decrease in the contribution of the neutrons at spin 8^+ . At spin

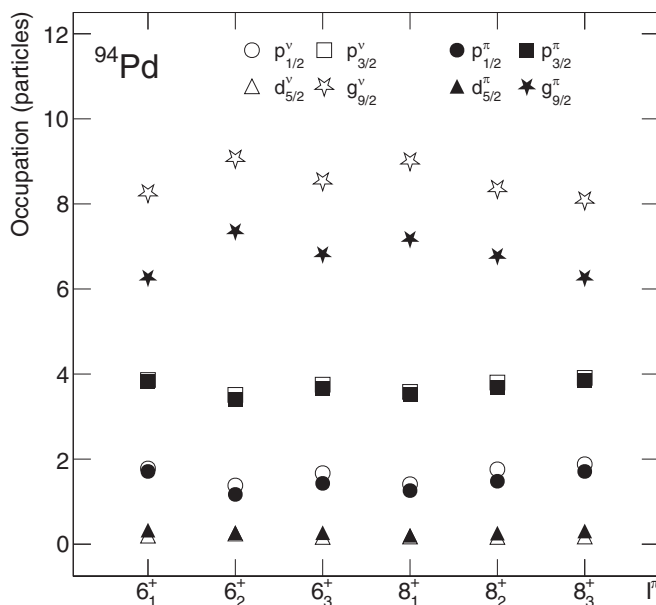


FIG. 3. Same as in Fig. 3, but for the lowest three 6^+ and 8^+ states in ^{94}Pd .

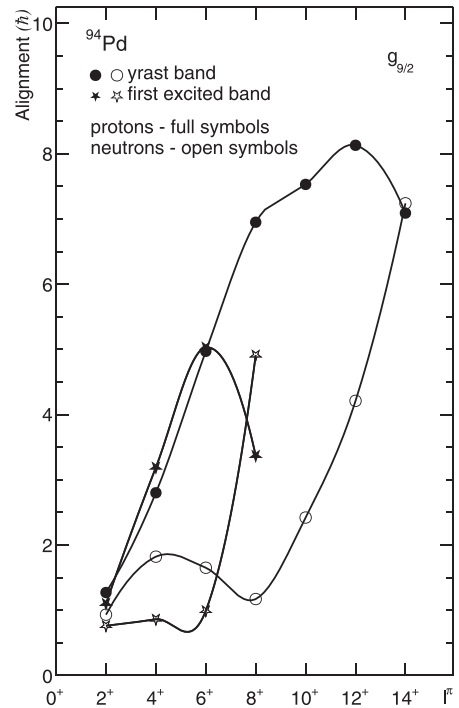


FIG. 4. The alignment plot for the yrast band and the first excited band in ^{94}Pd .

10^+ and 12^+ one can observe a fast alignment on the neutron side and a small increment in the proton alignment. At the 14^+ isomer the neutron alignment is drastically increased, while the proton alignment is decreasing. For the first excited band the behavior is similar to the one manifested for the yrast band up to spin 6^+ , but at spin 8^+ a strong alignment of the neutrons and a decrease in the alignment of the protons is displayed. It is worthwhile to mention that for the third 8^+ the alignment indicates values between the ones obtained for the first two 8^+ states. The alignment plot is corroborated by the calculated g factors. For the lowest three 8^+ states the calculated EXVAM g factors amount to $g(8_1^+) = 1.22$, $g(8_2^+) = 0.37$, and $g(8_3^+) = 0.70$, while with increasing spin we obtained $g(10_1^+) = 1.03$, $g(12_1^+) = 0.85$, and $g(14_1^+) = 0.53$.

B. β decay of the 0^+ ground state and the 7^+ isomer in ^{94}Ag

As mentioned in the Introduction, this work aims to achieve a simultaneous description of the properties of the investigated states in ^{94}Pd and their feeding by the β decay of the neighboring nucleus ^{94}Ag within the same theoretical framework. We investigated the superallowed Fermi β decay of the 0^+ ground state as well as the Gamow-Teller β decay of the 7^+ isomer in ^{94}Ag . The wave function for the ground state of ^{94}Ag independently built using a 30-dimensional EXVAM basis indicates a 95% oblate content, similar to the ground state of ^{94}Pd . For the study of the superallowed Fermi decay the dimension of the EXVAM basis for the description of the daughter 0^+ states in the β window in ^{94}Pd was extended to 30. The 7^+ isomer in ^{94}Ag was obtained building 14 EXVAM configurations, and the wave function for this state is based mainly on oblate deformed configurations, the two main ones

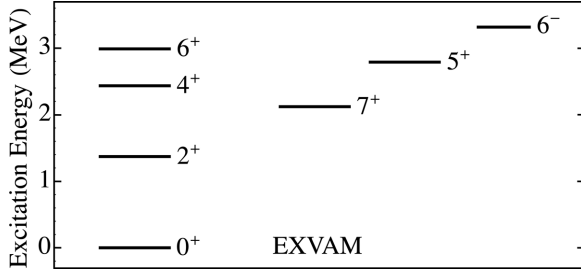


FIG. 5. Complex excited Vampir low-lying states in ^{94}Ag (see text for details).

making 91% of the total amplitude. The EXVAM excitation energy of the 7^+ isomer, situated below the yrast 5^+ and 6^+ states dominated by prolate deformed configurations and the yrast 6^- state dominated by oblate ones, amounts to 2.118 MeV, as illustrated in Fig. 5. The calculated spectroscopic quadrupole moment for the 7^+ isomer is $75.8 e\text{fm}^2$ and the g -factor value is 0.54. For the daughter 6^+ and 8^+ states in the β window up to 33 EXVAM configurations in ^{94}Pd were constructed.

The Fermi and Gamow-Teller reduced transition probabilities treated on the same footing are written as

$$B_{if}(F) = \frac{1}{2J_i + 1} |M_F|^2, \quad (1)$$

$$B_{if}(\text{GT}) = \frac{1}{2J_i + 1} \left(\frac{g_A}{g_V} \right)^2 |M_{\text{GT}}|^2, \quad (2)$$

where $g_A/g_V = -1.26$. The Fermi and Gamow-Teller nuclear matrix elements between the initial ($|\xi_i J_i\rangle$) and the final ($|\xi_f J_f\rangle$) states of spin J_i and J_f ($\xi_{i(f)}$ denotes all the other quantum numbers), respectively,

$$\begin{aligned} M_F &\equiv (\xi_f J_f || \hat{1} || \xi_i J_i) \\ &= \delta_{J_i J_f} \sum_{ab} M_F(ab) (\xi_f J_f || [c_a^{\nu\dagger} \tilde{c}_b^\pi]_0 || \xi_i J_i), \end{aligned} \quad (3)$$

$$\begin{aligned} M_{\text{GT}} &\equiv (\xi_f J_f || \hat{\sigma} || \xi_i J_i) \\ &= \sum_{ab} M_{\text{GT}}(ab) (\xi_f J_f || [c_a^{\nu\dagger} \tilde{c}_b^\pi]_1 || \xi_i J_i), \end{aligned} \quad (4)$$

are composed of the reduced single-particle matrix elements of the unit operator $\hat{1}$, $M_F(ab) = (a || \hat{1} || b)$, and Pauli spin operator $\hat{\sigma}$, $M_{\text{GT}}(ab) = 1/\sqrt{3} (a || \hat{\sigma} || b)$, and the reduced one-body transition densities calculated using the harmonic oscillator wave functions. For the β^+ decay and electron capture, $c_a^{\nu\dagger}$ is the neutron creation operator and \tilde{c}_b^π is the proton annihilation operator and the sum runs over the valence nucleons.

Figure 6 shows the Fermi strength distribution for the decay of the 0^+ ground state of ^{94}Ag to 0^+ states in ^{94}Pd . The results indicate that the depletion of the ground to ground transition amounts to 1.32% with the missing strength distributed over many 0^+ states, the strongest populated one being the third 0^+ state dominated by prolate deformed EXVAM configurations (94%). It is worthwhile to mention that the value of 1.32% represents the isospin-symmetry-breaking correction,

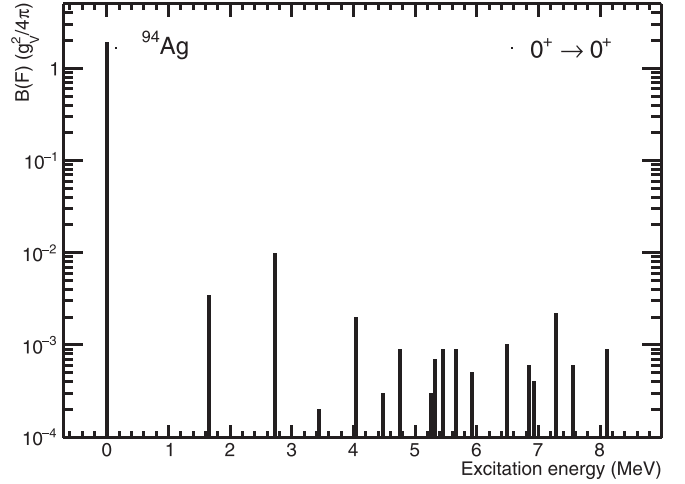


FIG. 6. The Fermi strength distribution for the decay of the 0^+ ground state in ^{94}Ag obtained within the complex excited Vampir model.

but one cannot disentangle between the effects of the isospin-symmetry-breaking interactions and shape mixing.

Figures 7 and 8 present the spectroscopic quadrupole moments of the calculated 6^+ and 8^+ Gamow-Teller daughter states in ^{94}Pd , respectively, illustrating the evolution of shape coexistence and mixing with increasing excitation energy. The structure of the wave functions for the 6^+ states in ^{94}Pd that display a small spectroscopic quadrupole moment indicates strong prolate-oblate mixing. A similar evolution of shape coexistence and mixing with increasing excitation energy is manifested in the structure of the 8^+ Gamow-Teller daughter states in ^{94}Pd , as can be seen from Fig. 8. Figures 9 and 10 depict the Gamow-Teller strength distribution for the decay of the 7^+ isomer in ^{94}Ag to 6^+ and 8^+ states in ^{94}Pd , respectively. The excitation energy of the yrast 6^+ and 8^+ states is slightly changed to the experimental value (the shifts amount to 449 and 176 keV for the 6^+ and 8^+ states, respectively), while

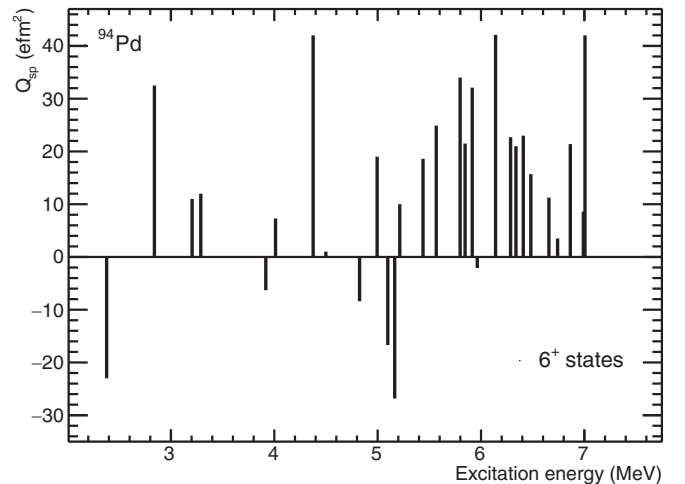
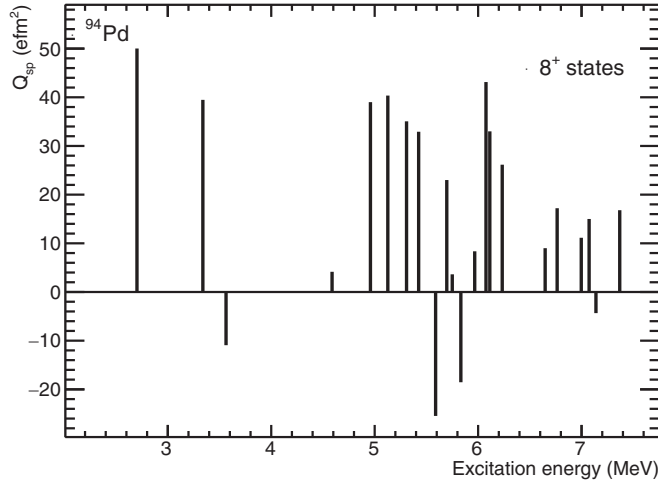
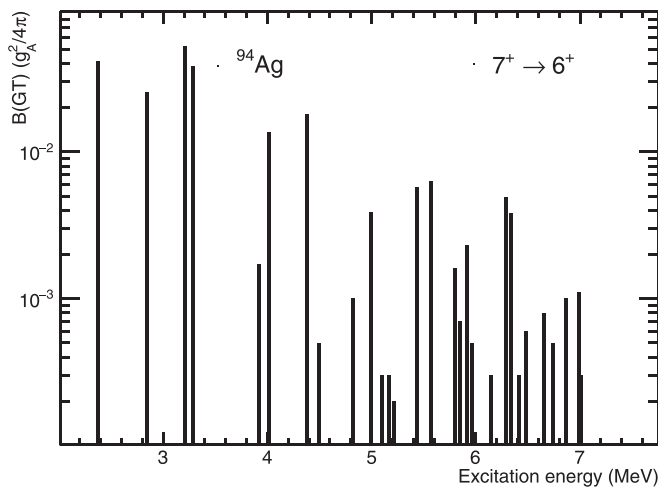
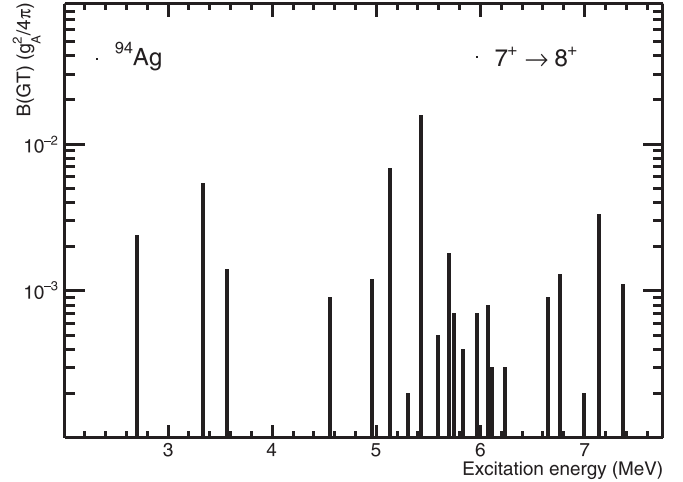


FIG. 7. Spectroscopic quadrupole moments of 6^+ Gamow-Teller daughter states in ^{94}Pd .

FIG. 8. Same as in Fig. 6, but for 8^+ states in ^{94}Pd .

for the excited states the relative value with respect to the yrast ones are considered. Very weak transition strengths were found for the decay of the 7^+ isomer to 7^+ states in ^{94}Pd . The contribution to the half-life of the 7^+ isomer brought by the decay to 7^+ states is one order of magnitude weaker than the one produced by the decay to 8^+ states.

The analysis of the structure of the strongest Gamow-Teller branches feeding the 6^+ states indicates dominant contribution coming from the $0g_{9/2}^v 0g_{9/2}^\pi$ matrix elements. Smaller coherent contributions are brought by the $1d_{5/2}^v 1d_{5/2}^\pi$ and $1p_{1/2}^v 1p_{3/2}^\pi$ matrix elements. The structure of the strongest Gamow-Teller branches feeding the 8^+ states show contribution from the $0g_{9/2}^v 0g_{9/2}^\pi$ matrix elements or small coherent contributions from $1p_{1/2}^v 1p_{3/2}^\pi$, $1p_{3/2}^v 1p_{1/2}^\pi$, and $1p_{3/2}^v 1p_{3/2}^\pi$ matrix elements. The Gamow-Teller accumulated strengths for the decay of the 7^+ isomer to the 6^+ and 8^+ states in ^{94}Pd is shown in Fig. 11. We calculated the β -delayed proton emission probability taking into account the contributions from

FIG. 9. The Gamow-Teller strength distribution for the decay of the 7^+ isomer in ^{94}Ag to 6^+ states in ^{94}Pd obtained within the *complex excited Vampir* model.FIG. 10. Same as in Fig. 8, but for 8^+ states in ^{94}Pd .

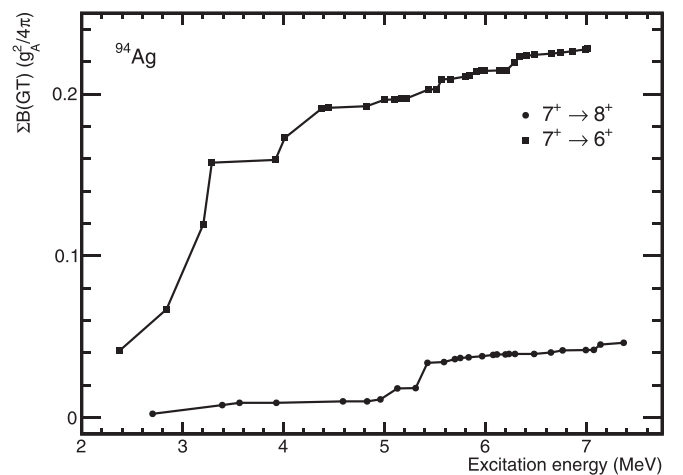
the 6^+ and 8^+ states with excitation energy higher than one-proton separation energy in the daughter nucleus, S_p (4.378 MeV) [29]:

$$P_p = \frac{\sum_{S_p}^{Q_{EC}} f(Z, E_f) B(\text{GT}, E_f)}{\sum_0^{Q_{EC}} f(Z, E_f) B(\text{GT}, E_f)}. \quad (5)$$

The calculated EXVAM value amounts to 27%, indicating rather good agreement with the experimental value of 20% [1]. The half-life for the 7^+ isomer is given by

$$\frac{1}{T_{1/2}} = \frac{1}{K} \sum_{E_f} f(Z, E_f) B_{if}(\text{GT}), \quad (6)$$

where E_f denotes the energy of the final state, $K = 6146$ s, and the Fermi integrals $f(Z, E_f)$ are taken from Ref. [31]. We considered the β window for the 7^+ isomer decay as $Q_{EC} = 14.4$ MeV, taking into account the ground to ground window $Q_{EC} = 13.7$ (4) MeV and $S_p = 0.700$ (5) MeV for ^{94}Ag [29,32]. The *complex excited Vampir* result for the half-

FIG. 11. The *complex excited Vampir* Gamow-Teller accumulated strength for the decay of the 7^+ isomer in ^{94}Ag to 6^+ and 8^+ states in ^{94}Pd .

life of the 7^+ isomer amounts to 0.28 s (quenching was not introduced), while the experimental value of 0.55(6) s [29] is almost two times longer. It is worthwhile to mention that the present results on the Gamow-Teller strength distributions could be changed, at least for the high excitation energy region, by the higher-lying configurations not included in the *complex* excited Vampir many-nucleon basis. Of course, changes in the renormalization of the effective interaction could influence the shape mixing in the structure of the wave functions of parent and daughter states. We are currently extending our studies to other proton-rich nuclei in the mass region to establish improvements required to solve the mentioned discrepancies with respect to the available data. Of course, experimental Gamow-Teller strength distributions for the decay of the 7^+ isomer in ^{94}Ag could help these theoretical investigations.

IV. CONCLUSIONS

This work presents the first comprehensive study on the structure and dynamics of the positive parity states up to spin 14^+ in the ^{94}Pd nucleus revealing, the nature of the isomeric states at spin 8^+ and 14^+ and the feeding by β decay of

the neighboring nucleus ^{94}Ag within the beyond-mean-field *complex* excited Vampir model. The structure and electromagnetic properties of the states in ^{94}Pd as well as the Gamow-Teller β decay of the 7^+ isomer and the superallowed Fermi β decay of the 0^+ ground state of ^{94}Ag have been described within the same theoretical framework using the same effective interaction and model space. The evolution of shape coexistence and mixing with increasing spin and excitation energy corroborated with the change in the alignment of the protons and neutrons occupying the $0g_{9/2}$ spherical orbital are responsible for the isomeric nature of the yrast 8^+ and 14^+ states. The observed decay pattern of the lowest 6^+ and 8^+ states in ^{94}Pd populated in the Gamow-Teller β decay of the 7^+ isomer in ^{94}Ag is supported by the predicted changes in the shape mixing. The comparison with the available experimental data indicates rather good agreement and supports our scenario on the evolution of the shape coexistence and mixing in the ^{94}Pd nucleus.

ACKNOWLEDGMENTS

This work was supported by a grant of the Ministry of Research, Innovation and Digitization, CNCS - UEFISCDI, Project No. PN-III-P4-PCE-2021-0060, within PNCDI III.

-
- [1] I. Mukha *et al.*, *Phys. Rev. C* **70**, 044311 (2004).
 - [2] I. Mukha *et al.*, *Nature (London)* **439**, 298 (2006).
 - [3] B. Cederwall *et al.*, *Nature (London)* **469**, 68 (2011).
 - [4] B. S. Nara Singh *et al.*, *Phys. Rev. Lett.* **107**, 172502 (2011).
 - [5] S. Zerguine and P. Van Isacker, *Phys. Rev. C* **83**, 064314 (2011).
 - [6] B. S. Nara Singh *et al.*, *Phys. Rev. C* **86**, 041301(R) (2012).
 - [7] C. B. Hinke *et al.*, *Nature (London)* **486**, 341 (2012).
 - [8] G. J. Fu, J. J. Shen, Y. M. Zhao, and A. Arima, *Phys. Rev. C* **87**, 044312 (2013).
 - [9] K. Moschner *et al.*, *EPJ Web Conf.* **93**, 01024 (2015).
 - [10] P. J. Davies *et al.*, *Phys. Rev. C* **99**, 021302(R) (2019).
 - [11] J. Park *et al.*, *Phys. Rev. C* **99**, 034313 (2019).
 - [12] B. Cederwall *et al.*, *Phys. Rev. Lett.* **124**, 062501 (2020).
 - [13] H. Schatz, A. Aprahamian, V. Barnard, L. Bildsten, A. Cumming, M. Ouellette, T. Rauscher, F. K. Thielemann, and M. Wiescher, *Phys. Rev. Lett.* **86**, 3471 (2001).
 - [14] R. Gross and A. Frenkel, *Nucl. Phys. A* **267**, 85 (1976).
 - [15] K. Schmidt *et al.*, *Nucl. Phys. A* **624**, 185 (1997).
 - [16] H. Herndl and B. A. Brown, *Nucl. Phys. A* **627**, 35 (1997).
 - [17] M. La Commara *et al.*, *Nucl. Phys. A* **708**, 167 (2002).
 - [18] C. Plettner *et al.*, *Nucl. Phys. A* **733**, 20 (2004).
 - [19] T. S. Brock *et al.*, *Phys. Rev. C* **82**, 061309(R) (2010).
 - [20] P. H. Regan, in *SSNET2022, Shapes and Symmetries in Nuclei: from Experiment to Theory*, Orsay, France, May–June 2022 (unpublished).
 - [21] A. Petrovici, K. W. Schmid, O. Radu, and A. Faessler, *Phys. Rev. C* **78**, 064311 (2008).
 - [22] M. Honma, T. Otsuka, T. Mizusaki, and M. Hjorth-Jensen, *Phys. Rev. C* **80**, 064323 (2009).
 - [23] A. Obertelli *et al.*, *Phys. Rev. C* **80**, 031304(R) (2009).
 - [24] A. Obertelli *et al.*, *Phys. Lett. B* **701**, 417 (2011).
 - [25] K. Heyde and J. L. Wood, *Rev. Mod. Phys.* **83**, 1467 (2011).
 - [26] A. Petrovici, *Phys. Rev. C* **91**, 014302 (2015).
 - [27] A. Petrovici, *Phys. Rev. C* **97**, 024313 (2018).
 - [28] K. Wimmer *et al.*, *Eur. Phys. J. A* **56**, 159 (2020).
 - [29] <http://www.nndc.bnl.gov>.
 - [30] J. Park *et al.*, *Phys. Rev. C* **96**, 044311 (2017).
 - [31] N. B. Gove and M. J. Martin, *At. Data Nucl. Data Tables* **10**, 205 (1971).
 - [32] M. Wang *et al.*, *Chin. Phys. C* **36**, 1603 (2012).